OMICS A Journal of Integrative Biology
Volume 25, Number 12, 2021

DOI: 10.1089/omi.2021.0097

Open camera or QR reader and scan code to access this article and other resources online.

Discovery of Cancer-Specific and Independent Prognostic Gene Subsets of the Slit-Robo Family Using TCGA-PANCAN Datasets

Ayse Ozhan,[1] Melike Tombaz,[2] and Ozlen Konu[1–3,i]

Abstract

The Slit-Robo family of axon guidance molecules works in concert, playing important roles in organ development and cancer. Expressions of individual Slit-Robo genes have been used in calculating univariable hazard ratios (HR_{uni}) for predicting cancer prognosis in the literature. However, Slit-Robo members do not act independently; hence, hazard ratios from multivariable Cox regression (HR_{multi}) on the whole gene set can further lead to identification of cancer-specific, novel, and independent prognostic gene pairs or modules. Herein, we obtained mRNA expressions of the Slit-Robo family consisting of four Robos (*ROBO1/2/3/4*) and three Slits (*SLIT1/2/3*), along with four types of survival outcome across cancers found in the Cancer Genome Atlas (TCGA). We used cluster heat maps to visualize closely associated pairs/modules of prognostic genes across 33 different cancers. We found a smaller number of significant genes in HR_{multi} than in HR_{uni}, suggesting that the former analysis was less redundant. High *ROBO4* expression emerged as relatively protective within the family, in both types of HR analyses. Multivariable Cox regression, on the other hand, revealed significantly more HR signatures containing Slit-Robo pairs acting in opposing directions than those containing Slit-Slit or Robo-Robo pairs for disease-specific survival. Furthermore, we discovered, through the online app SmulTCan's lasso regression, Slit-Robo gene subsets that significantly differentiated between high- versus low-risk prognosis patient groups, particularly for renal cancers and low-grade glioma. The statistical pipeline reported herein can help test independent and significant pairs/modules within a codependent gene family for cancer prognostication, and thus should also prove useful in personalized/precision medicine research.

Keywords: cancer, biomarkers, Slit-Robo, prognosis, gene expression, personalized medicine

Introduction

Initially discovered in the nervous system, the Slit-Robo pathway has been the focus of recent research due to its role in organ development (Blockus and Chedotal, 2016), as well as tumor progression and angiogenesis in several human cancers (Tong et al., 2019). Slits are large, secreted proteins, whose axonal repulsive activities are mediated by receptors of the Roundabout (Robo) family. The three Slit and four Robo genes are known to act in pairs/modules (Carr et al., 2017; Wu et al., 2001) and might be co-expressed tissue specifically.

For instance, in liver cancer, Slit-Robo members form two distinct co-expression modules, splitting into clusters of *ROBO1-ROBO2-SLIT1* and *ROBO4-SLIT2-SLIT3* (Avci et al., 2008). In others, the *ROBO1-SLIT2* pair emerges frequently, for example, in breast cancer, *ROBO1* as well as

[1]UNAM-National Nanotechnology Research Center, Institute of Material Science and Nanotechnology, Bilkent University, Ankara, Turkey.
[2]Department of Molecular Biology and Genetics, Faculty of Science, Bilkent University, Ankara, Turkey.
[3]Interdisciplinary Graduate Program in Neuroscience, Aysel Sabuncu Brain Research Center, Bilkent University, Ankara, Turkey.
[i]ORCID ID (https://orcid.org/0000-0002-6223-5329).

ROBO2 are present while deeming *SLIT2* a potential chemoattractant (Choi et al., 2014; Qin et al., 2015; Rezniczek et al., 2019).

In gastric cancer, *ROBO1* and *SLIT2* are both downregulated (Xia et al., 2019), while *SLIT2,* upregulated in renal cell tumors, is expressed by human embryonic kidney cells where *ROBO1* activation leads to malignancy (Ho et al., 2017; Zhou et al., 2011). In addition to these, *SLIT2* can pair with *ROBO3* in regulation of the migration of Gonadotropin-releasing hormone (GnRH) neurons (Cariboni et al., 2012), and with *ROBO4* in inhibition of pathological neovascularization in the retina (Jones et al., 2009). On the other hand, the *SLIT3-ROBO4* pair can promote angiogenesis and vascularization in engineered stem cells (Paul et al., 2013).

The abovementioned findings strongly indicate that Slit-Robo pairs/modules may function as oncogenes or tumor suppressors cancer and tissue specifically. Indeed, previous studies have associated the misexpression of Slit-Robo pathway members with prognostic significance in multiple cancers primarily through univariable survival analyses (Schmid et al., 2007; Xia et al., 2019; Zhang et al., 2015). However, there is not yet a pan-cancer Slit-Robo family analysis using multivariable Cox regression, which can provide cancer-specific independent prognostic signatures.

Survival analyses performed on gene sets report univariable as well as multivariable estimates using Kaplan–Meier (K-M) plots and tables of HR (Chen et al., 2020; Meng et al., 2020). Most often, the univariable estimates are primarily used to filter genes before the multivariable analysis and reduce the size of the gene set (Wu et al., 2020). Obtaining risk scores [e.g., RNA processing genes in colorectal cancer (Lu et al., 2020)] as well as predicting the best subsets of a given gene set (e.g., netrins and their receptors (Ozhan et al., 2021)) are among many advantages of using multivariable Cox regression models.

Herein we report the hazard ratio estimates (HR_{uni} and HR_{multi}) of univariable and multivariable Cox regression using Slit-Robo pathway expression from the Cancer Genome Atlas's Pan-Cancer (TCGA-PANCAN) dataset (Gao et al., 2019) obtained from UCSC Xena (Goldman et al., 2020). Both HR_{uni} and HR_{multi} estimates identified *ROBO4* expression as the most protective, while the HR_{multi} signatures of Slit-Robo pairs acting in opposite directions were more common than any other Slit-Robo, Slit-Slit, or Robo-Robo pairs. These findings suggest that Slits and Robos may balance each other in their expression, and/or those that pair may work together.

Moreover, a median prognostic index (PI) calculated from Slit-Robo models using SmulTCan (Ozhan et al., 2021) successfully differentiated between high- and low-risk groups for several cancers, including those of the kidney and low-grade glioma. Our findings implicate that gene families that exhibit interdependence, such as Slit-Robo, can benefit from multivariable Cox regression to establish the most influential and independent family members.

Materials and Methods

Computation of HR matrices

The results shown in this study are in whole or in part based upon data generated by TCGA Research Network: https://www.cancer.gov/tcga/.

The TCGA-PANCAN TSV file containing normalized RNA-Seq expression values of the four Robos and the three Slits was obtained from UCSC Xena (http://xena.ucsc.edu). This file contained tissue samples across 33 TCGA datasets for the Slit-Robo genes (https://portal.gdc.cancer.gov). Primary (or primary blood derived for LAML) tumor samples for each survival type, that is, overall survival (OS), disease-specific survival (DSS), disease-free survival (DFS), and progression-free survival (PFS), were separately analyzed with Cox regression.

The ''UCSCXenaTools'' Bioconductor package (Wang and Liu, 2019) was used to download survival TXT files of each of the datasets from TCGA. Sample sizes of each dataset consisting of primary tumors in the downloaded PANCAN file from Xena having expression values of all Slit-Robo members are shown in Supplementary Table S1; these samples were used in multivariable Cox regression and best-subset coefficient computations.

The SmulTCan's statistical pipeline was adopted to calculate the HR_{uni} and HR_{multi} values as described previously (Ozhan et al., 2021). Briefly, an HR and its associated *p*-value were calculated for each of the seven Slit-Robo genes in each cancer dataset from both univariable and multivariable Cox regressions, using the coxph() function of the ''survival'' package in R (Therneau and Grambsch, 2000). This function was also used in calculating low:high risk ratios of the PI analyses (Ozhan et al., 2021).

Datasets GBM, SKCM, THYM, and UVM were excluded from both univariable and multivariable DFS analyses, due to absence of information regarding DFS. THYM was excluded from the DSS, while KICH and MESO were excluded from the DFS analyses due to multivariable models not converging. The LAML dataset was used only in the univariable Slit-Robo analyses for OS, since it lacks data for the remaining survival types.

Statistical comparison of univariable and multivariable Cox regression results

We summarized, with a workflow diagram, the steps of statistical comparisons performed between the HR_{uni} and HR_{multi} matrices where the rows represented the cancers, and the columns each of the seven Slit-Robo family members (Supplementary Fig. S1). Euclidean distances of HR_{uni} and HR_{multi} matrices were calculated with the default parameters of dist() in R. To equalize matrix dimensions for each survival type, the corresponding dataset in HR_{uni} was removed for which there were no HR_{multi} entries. Datasets excluded from HR_{uni} matrices were LAML in OS and PFS; LAML and THYM for DSS; and GBM, SKCM, THYM, UVM, LAML, KICH, and MESO for DFS.

HR_{uni} and HR_{multi} matrices were then compared using the Mantel test to identify the correlation between these matrices by the ''cultevo'' package with the Spearman method (Stadler, 2018); and the correlation constant $r \pm$ the standard error (SE) was reported. Differences between element-wise Euclidean distances of HR_{uni} and those of HR_{multi} from Cox regressions were obtained for each Slit-Robo member in each survival dataset and the box plots were drawn. The numbers of genes significant in HR_{uni} and HR_{multi}, separately, were calculated and tested in a pair-wise manner with the Wilcoxon signed-rank test. Finally, for each survival type, we calculated the χ^2 statistic and its *p*-value to test the significance of association between Slit-Robo (SR) or Slit-Slit/Robo-Robo (SS/RR) pairing and the direction of the HR. The analyses were carried out in the R v4.0.0 environment (www.r-project.org).

Data visualization

Visualization of univariable and multivariable Cox regression results with heat maps was achieved using packages ''gtools'' (Warnes et al., 2020) and ''heatmaply'' (Galili et al., 2018). The ''heatmaply'' package incorporating the hclust() function of R was used for hierarchical clustering with ''complete'' linkage. ''RColorBrewer'' (Neuwirth, 2014) and ''ggpubr'' (Kassambara, 2020) were used in coloring and arranging the positions of the plots.

In the heat maps, logarithmically transformed HR values ($\log_2$HR) were used for symmetricity and generating a visual summary of the clustering patterns of Slit-Robo genes as well as different cancers. For forest plots, the ggforest() function from ''survminer'' (Kassambara et al., 2020) was used and the results were provided as supplementary figures. Boxplots were generated using the geom_boxplot() function of ''ggplot2'' (Wickham, 2016). We provided the Slit-Robo expression TSV matrix for further analysis using the online tool SmulTCan.

Computation of PIs for the best subsets of the Slit-Robo pathway

The percent area under the receiver operating characteristics (ROC) curve (AUC) calculations was made with tools from the ''riskRegression'' package (Gerds and Ozenne, 2020). The cv.glmnet() function from ''glmnet'' was used to compute coefficients of Slit-Robo using lasso, with the ''nfolds'' parameter set to the sample size of each dataset and the ''family'' parameter set to ''cox''. A prognostic index (PI_i) for the *i*th sample in a cancer dataset was calculated as previously defined (Ozhan et al., 2021; Xue et al., 2019). Samples with a PI_i value greater than the median PI for the dataset were labeled as high risk, while remaining samples were deemed low risk. The survfit() function of ''survival'' was used to determine *p*-values of the K-M analyses.

Results

Comparison of HR_{uni} and HR_{multi} clusters of Slit-Robo family across TCGA datasets

Mantel's test provided a statistics for the comparison of HR_{uni} and HR_{multi} matrices of Slit-Robo members and indicated that the two matrices were significantly, but moderately correlated for OS ($r=0.68\pm0.14$, $p=0.01\times10^{-1}$), DSS ($r=0.71\pm0.15$, $p=0.01\times10^{-1}$), DFS ($r=0.75\pm0.16$, $p=0.01\times10^{-1}$), and PFS ($r=0.74\pm0.13$, $p=0.01\times10^{-1}$). However, the number of genes found significant in HR_{multi} was less than that in HR_{uni} (Table 1), suggesting the former was less redundant. Accordingly, both HR_{uni} and HR_{multi} identified the higher expression of *ROBO4* in association with better survival, in general.

The mean difference values between Euclidean distances of HR_{uni} and HR_{multi} estimates per gene were less than zero for all four survival types (Supplementary Fig. S2). This suggested that TCGA cancers became more similar among themselves according to the estimates of HR_{multi}. This was also supported by the shortened branch lengths among cancers in the heat map of HR_{multi} in each of the four survival types (Figs. 1–4) when compared with HR_{uni} (Supplementary Figs. S3 and S4).

Moreover, the topology of HR_{multi} heat map revealed that $\log_2$HR-based clustering distinctly grouped the TCGA cancers, given their prognostic similarities rather than just their Slit-Robo expression patterns, that is, the cancers within the same cluster had more similar HR estimates across the gene set and hence the prognostic signature (Figs. 1–4). This represents a relatively novel approach to investigate gene or cancer clustering in transcriptomics. Interestingly, we found that female cancers BRCA, OV, CESC, and UCEC frequently clustered together, while BLCA-LUSC, SARC-LIHC, KICH-PCPG, and KIRC-PAAD were among other cancers paired in two or more survival types (Figs. 1–4).

On the other hand, the cluster heat maps of HR_{multi} estimates column-wise provided more insight into which genes exhibited similar HR profiles. For OS, two main clusters, namely, *ROBO3-SLIT1-SLIT2-ROBO2* and *ROBO1-ROBO4-SLIT3*, emerged (Fig. 1). For DSS, the Slit-Robo family split into more prominent pairs, that is, *SLIT3-ROBO4*, *SLIT2-ROBO3*, and *SLIT1-ROBO2* (Fig. 2). For DFS, *ROBO1*, *ROBO2*, and *ROBO3*, each paired with a different Slit, *SLIT1*, *SLIT2*, and *SLIT3*, respectively, while *ROBO4* was found separately (Fig. 3). In PFS clustering, again *ROBO4* diverged from the rest of the members, and *ROBO2-SLIT1-SLIT2* were more closely associated (Fig. 4).

HR_{multi} estimates visualized by heat maps helped summarize the prognostic gene clusters with independent effects for each of the four survival types. Interestingly, the heat map of HR_{multi} estimates consisted of more pairs/modules with

Table 1. Number of Significant Genes ($p<0.05$) for Univariable and Multivariable Analysis Results for Each Gene in Each Survival Type

	OS		*DSS*		*DFS*		*PFS*	
	Uni	*Multi*	*Uni*	*Multi*	*Uni*	*Multi*	*Uni*	*Multi*
ROBO1	5	2	7	3	4	1	5	4
ROBO2	5	4	8	6	3	2	10	5
ROBO3	5	6	6	5	2	2	4	3
ROBO4	8	7	6	7	2	1	6	6
SLIT1	7	3	8	4	4	2	7	3
SLIT2	4	2	5	4	4	3	5	4
SLIT3	6	4	5	4	4	3	6	3
Wilcoxon signed-rank *p*-value	0.050		0.058		0.031		0.034	

The number of significant genes in the univariable and multivariable analyses was pair-wise compared for each gene, and the Wilcoxon signed-rank *p*-values have been indicated for each survival type.

DFS, disease-free survival; DSS, disease-specific survival; Multi, multivariable; OS, overall survival; PFS, progression-free survival; Uni, univariable.

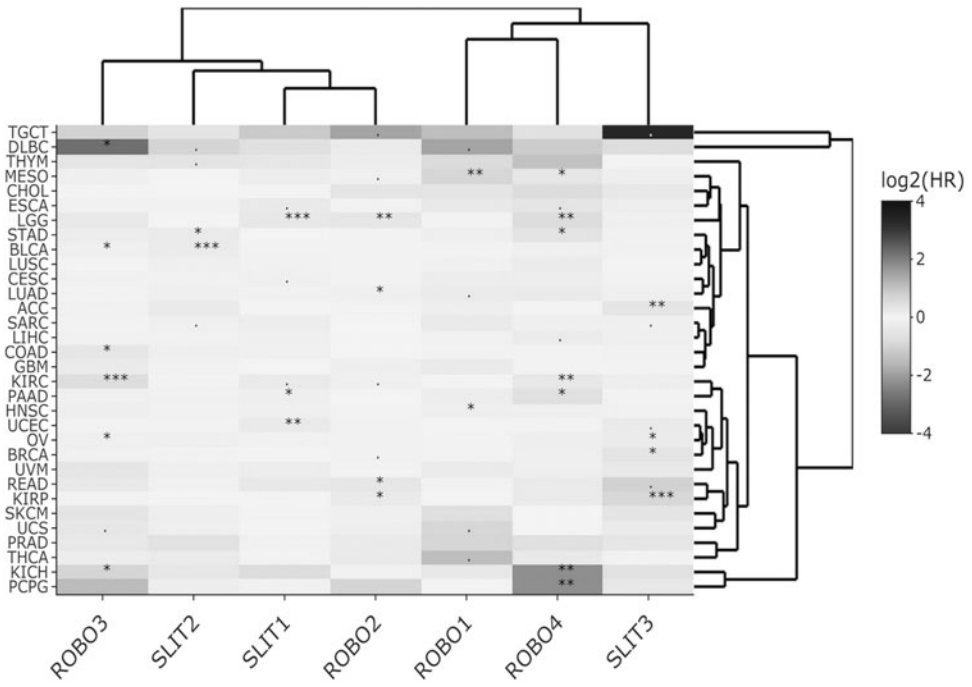

FIG. 1. Heat map of Slit-Robo OS $\log_2$HR values across TCGA datasets for multivariable Cox regression. Significant HR associations are indicated with *** for $p < 0.001$, ** for $p < 0.01$, * for $p < 0.05$, and $^+$ for $p < 0.1$. HR, hazard ratio; OS, overall survival.

members from both Slit and Robo (Figs. 1–4) when compared with the HR_{uni} heat maps (Supplementary Figs. S3 and S4). Moreover, the Slit-Robo pairs in opposing HR directions (>1 and <1 or <1 and >1) were observed more often than Slit-Slit or Robo-Robo pairs in either direction ($\chi^2 \cong 5.49$, $p < 0.05$; Supplementary Table S2).

Discovery of independent Slit-Robo pairs across groups of TCGA cancers

Significant HR_{multi} results showed that several cancers had two or more Slit-Robo members simultaneously and independently implicated in prognosis (Tables 2 and 3). We

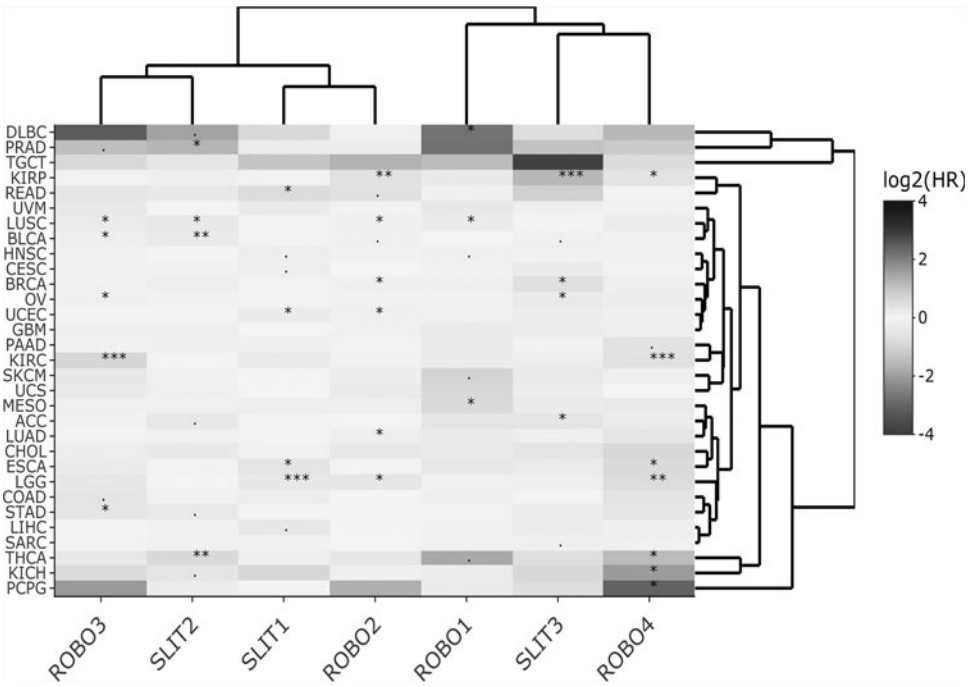

FIG. 2. Heat map of Slit-Robo DSS $\log_2$HR values across TCGA datasets for multivariable Cox regression. Significant HR associations are indicated with *** for $p < 0.001$, ** for $p < 0.01$, * for $p < 0.05$, and $^+$ for $p < 0.1$. DSS, disease-specific survival.

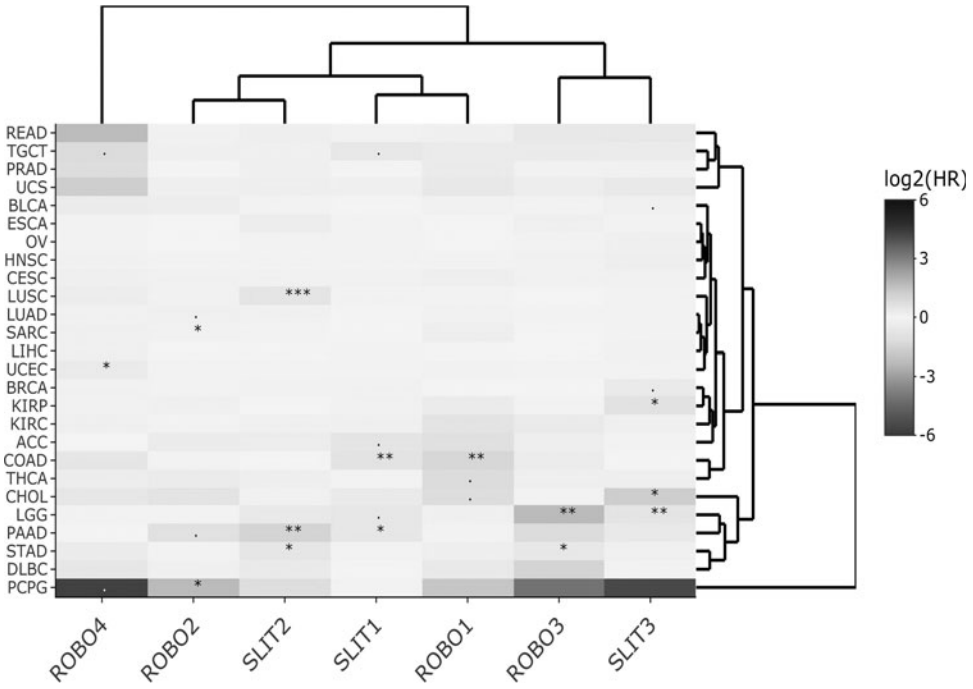

FIG. 3. Heat map of Slit-Robo DFS $\log_2$HR values across TCGA datasets for multivariable Cox regression. Significant HR associations are indicated with *** for $p < 0.001$, ** for $p < 0.01$, * for $p < 0.05$, and $^+$ for $p < 0.1$. DFS, disease-free survival.

highlighted below many of those recurrent Slit-Robo pairs/modules that were found to be significantly associated with prognosis of individual and/or groups of cancers in our multivariable analyses of TCGA datasets (Blum et al., 2018).

ROBO3, *ROBO4*. Multivariable Cox regression analysis of the kidney clear cell carcinoma (KIRC) exhibited one of the most significant prognostic pairs with respect to Slit-Robo signaling, such that a higher expression of *ROBO3*, and independently lower expression of *ROBO4,* indicated

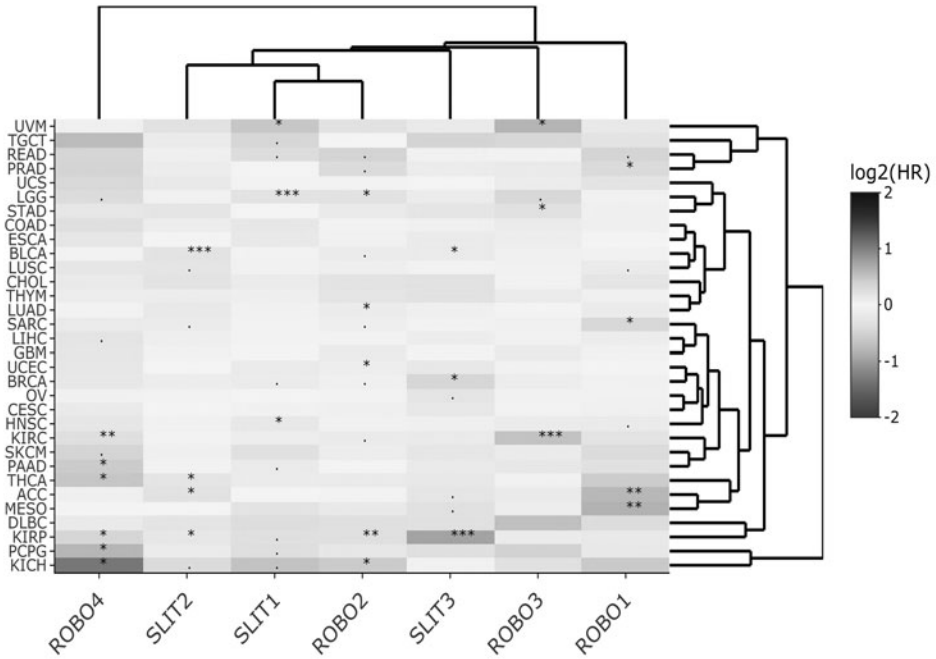

FIG. 4. Heat map of Slit-Robo PFS $\log_2$HR values across TCGA datasets for multivariable Cox regression. Significant HR associations are indicated with *** for $p < 0.001$, ** for $p < 0.01$, * for $p < 0.05$, and $^+$ for $p < 0.1$. PFS, progression-free survival.

Table 2. Slit-Robo HR Values Resulting from Multivariable Cox Regression Are Given for Those HRs with $P < 0.05$, for Survival Types OS and DSS in the Investigated TCGA Datasets

	ROBO1		*ROBO2*		*ROBO3*		*ROBO4*		*SLIT1*		*SLIT2*		*SLIT3*	
	OS	*DSS*	*OS*	*DSS*	*OS*	*DSS*	*OS*	*DSS*	*OS*	*DSS*	*OS*	*DSS*	*OS*	*DSS*
ACC	—	—	—	—	—	—	—	—	—	—	—	—	0.73	0.73
BLCA	—	—	—	—	0.89	0.87	—	—	—	—	1.14	1.14	—	—
BRCA	—	—	—	0.91	—	—	—	—	—	—	—	—	1.27	1.37
COAD	—	—	—	—	1.24	—	—	—	—	—	—	—	—	—
DLBC	—	4.48	—	—	0.14	—	—	—	—	—	—	—	—	—
ESCA	—	—	—	—	—	—	—	1.47	—	1.26	—	—	—	—
HNSC	0.86	—	—	—	—	—	—	—	—	—	—	—	—	—
KICH	—	—	—	—	1.60	—	0.21	0.25	—	—	—	—	—	—
KIRC	—	—	—	—	1.41	1.55	0.76	0.63	—	—	—	—	—	—
KIRP	—	—	0.80	0.65	—	—	—	0.66	—	—	—	—	1.52	2.24
LGG	—	—	1.22	1.20	—	—	1.44	1.43	0.76	0.76	—	—	—	—
LUAD	—	—	0.90	0.88	—	—	—	—	—	—	—	—	—	—
LUSC	—	0.83	—	0.88	—	0.84	—	—	—	—	—	1.19	—	—
MESO	1.56	1.47	—	—	—	—	1.23	—	—	—	—	—	—	—
OV	—	—	—	—	0.89	0.88	—	—	—	—	—	—	1.12	1.16
PAAD	—	—	—	—	—	—	0.64	—	0.87	—	—	—	—	—
PCPG	—	—	—	—	—	—	0.21	0.12	—	—	—	—	—	—
READ	—	—	0.72	—	—	—	—	—	—	1.42	—	—	—	—
STAD	—	—	—	—	—	1.22	1.29	—	—	—	1.15	—	—	—
THCA	—	—	—	—	—	—	—	0.35	—	—	—	0.55	—	—
UCEC	—	—	—	0.89	—	—	—	—	1.15	1.14	—	—	—	—

Refer to Supplementary Table S1 for cancer dataset abbreviations.
HR, hazard ratio; TCGA, The Cancer Genome Atlas.

worse prognosis in KIRC patients for OS, DSS, and PFS, but not DFS, while the effects of remaining Slit-Robo members were insignificant (Supplementary Fig. S5). Similarly, the HR_{multi} profile indicating a hazardous expression of *ROBO3* and a protective one for *ROBO4* was observed for OS (but not in the other survival types) in chromophobe renal cell (KICH) carcinoma (Supplementary Fig. S6).

SLIT3, ROBO2/ROBO4. Unlike KIRC and KICH, the papillary cell renal carcinoma KIRP exhibited a relatively

Table 3. Slit-Robo HR Values Resulting from Multivariable Cox Regression Are Given for Those HRs with $P < 0.05$, for Survival Types DFS and PFS in the Investigated TCGA Datasets

	ROBO1		*ROBO2*		*ROBO3*		*ROBO4*		*SLIT1*		*SLIT2*		*SLIT3*	
	DFS	*PFS*	*DFS*	*PFS*	*DFS*	*PFS*	*DFS*	*PFS*	*DFS*	*PFS*	*DFS*	*PFS*	*DFS*	*PFS*
ACC	—	1.49	—	—	—	—	—	—	—	—	—	1.14	—	—
BLCA	—	—	—	—	—	—	—	—	—	—	—	1.14	—	0.90
BRCA	—	—	—	—	—	—	—	—	—	—	—	—	—	1.25
COAD	—	—	—	—	—	—	—	—	—	—	—	—	0.31	—
DLBC	1.95	—	—	—	—	—	—	—	1.47	—	—	—	—	—
HNSC	—	—	—	—	—	—	—	—	—	0.87	—	—	—	—
KICH	—	—	—	1.36	—	—	—	0.40	—	—	—	—	—	—
KIRC	—	—	—	—	—	1.42	—	0.78	—	—	—	—	1.53	—
KIRP	—	—	—	0.79	3.25	—	—	0.72	—	—	—	0.85	0.56	1.67
LGG	—	—	—	1.14	—	—	—	—	—	0.82	—	—	—	—
LUAD	—	—	—	0.90	—	—	—	—	—	—	—	—	—	—
LUSC	—	—	—	—	—	—	—	—	—	—	1.40	—	—	—
MESO	—	1.54	—	—	—	—	—	—	—	—	—	—	—	—
PAAD	—	—	—	—	—	—	—	0.67	0.64	—	2.06	—	—	—
PCPG	—	—	0.21	—	—	—	—	0.57	—	—	—	—	—	—
PRAD	—	0.75	—	—	—	—	—	—	—	—	—	—	—	—
SARC	—	1.24	0.89	—	—	—	—	—	—	—	—	—	—	—
SKCM	—	—	—	—	1.31	—	—	—	—	—	1.37	—	—	—
STAD	—	—	—	—	—	1.16	—	—	—	—	—	—	—	—
THCA	—	—	—	—	—	—	—	0.64	—	—	—	0.82	—	—
UCEC	—	—	—	0.92	—	—	0.73	—	—	—	—	—	—	—
UVM	—	—	—	—	—	0.57	—	—	—	1.38	—	—	—	—

Refer to Supplementary Table S1 for cancer dataset abbreviations.

different pattern. In addition to the lower expression of *ROBO4* and that of *ROBO2*, a simultaneously higher expression of *SLIT3* was significantly associated with poor prognosis in DSS and PFS, but partly in OS and DFS (Supplementary Fig. S7). *SLIT3*'s higher expression accompanied by the decrease in *ROBO2* expression was a biomarker of poor prognosis also in the breast invasive carcinoma (TCGA-BRCA) dataset for DSS (but not for DFS or PFS; Supplementary Fig. S8).

SLIT2, ROBO4/ROBO3/SLIT3. In this study, HR_{multi} values of the stomach adenocarcinoma dataset (TCGA-STAD) indicated that the *SLIT2* and *ROBO4* pair could be significant in prognosis and behaved independently, yet in the same direction (i.e., increased) for OS, whereas *SLIT2* paired with *ROBO3* instead in DFS (Supplementary Fig. S9). Higher levels of *SLIT2* amidst lower levels of *ROBO3* were significantly associated with worse prognosis also in TCGA-BLCA, the bladder carcinoma for OS and DSS; although for PFS, high *SLIT2* levels were paired with low *SLIT3* (Supplementary Fig. S10). Similarly, a higher expression of *SLIT2*, instead of *SLIT3*, and lower expression of *ROBO3*, and *ROBO1 and ROBO2*, were associated with worse prognosis for DSS in TCGA-LUSC, the lung squamous cell carcinoma dataset (Supplementary Fig. S11).

SLIT2, SLIT1, ROBO1/ROBO4. Increased expression of *SLIT2* also indicated poor prognosis for PFS in TCGA-ACC, the adrenocortical cancer dataset, when together with that of *ROBO1* (Supplementary Fig. S12). However, increased *SLIT2* expression paired not with a Robo, but with decreased *SLIT1* expression in TCGA-PAAD, the pancreatic adenocarcinoma dataset, resulted in worse prognosis for DFS (Supplementary Fig. S13).

On the other hand, the decreased expression of *SLIT1* when combined with low *ROBO4* levels indicated a worse prognosis in TCGA-PAAD (Supplementary Fig. S13; for OS). The same could be concluded for decreased *SLIT2* with low *ROBO4* in TCGA-THCA, the thyroid carcinoma dataset (Supplementary Fig. S14; for DSS and PFS). Nevertheless, a high level of *SLIT1* was associated with worse prognosis in the esophageal cancer dataset TCGA-ESCA (Supplementary Fig. S15), as well as TCGA-COAD, the colorectal adenocarcinoma dataset (Supplementary Fig. S16). This hazardous effect of *SLIT1* expression was in combination with increased expression of *ROBO4* for DSS and that of *ROBO1* for DFS, in ESCA (Supplementary Fig. S15) and COAD (Supplementary Fig. S16), respectively.

SLIT1, ROBO2/ROBO3/ROBO4. As demonstrated in the cases above, our results showed that a Slit could pair simultaneously with one or more Robo genes and yet the same pair could exhibit opposite expression patterns in different cancers. For example, increased *SLIT1*, but decreased *ROBO2* indicated worse prognosis for DSS in TCGA-UCEC, the uterine corpus endometrial carcinoma, while the same was true for increased *SLIT1*, but decreased *ROBO3* for PFS in TCGA-UVM, the uveal melanoma dataset (Supplementary Figs. S17 and S18). On the contrary, decreased *SLIT1* along with increased *ROBO2* and *ROBO4* (instead of *ROBO3*) signified poor prognosis for TCGA-LGG, the low-grade glioma dataset (Supplementary Fig. S19; for OS and DSS).

SLIT3, ROBO3. Similarly, the same pair could be associated with different survival types in different cancers, yet in opposite manners as in the *SLIT3-ROBO3* pair for DFS in TCGA-LGG (Supplementary Fig. S19) and for DSS in TCGA-OV, the ovarian carcinoma dataset (Supplementary Fig. S20). Low *ROBO3* and high *SLIT3* levels were associated with DFS in TCGA-LGG (Supplementary Fig. S19), while the opposite was true for OS and DSS in TCGA-OV (Supplementary Fig. S20).

Others

Several cancers had a single Slit or Robo gene significantly associated with one or more survival types. For instance, the HR_{multi} profile of the Slit-Robo pathway in the lung adenocarcinoma dataset TCGA-LUAD showed that higher *ROBO2* expression was a significantly better predictor for OS, DSS, and PFS among lung adenoma patients, while other genes did not stand out as significant in any of the survival types (Supplementary Fig. S21).

Several other cancers, including TCGA-CHOL, the cholangioma dataset, exhibited significance for single genes rather than pairs (Supplementary Fig. S22). *ROBO4* expression was protective in the pheochromocytoma and paraganglioma dataset TCGA-PCPG (for OS, DSS, and PFS; Supplementary Fig. S23), and in the liver hepatocellular carcinoma dataset, TCGA-LIHC, verging on significance (PFS; $p < 0.1$; Supplementary Fig. S24). Nevertheless, none of the Slit-Robo pathway members was significantly implicated with prognosis in the GBM, TGCT, and THYM datasets (Tables 2 and 3).

Discovery of the best Slit-Robo subsets for prognostication

We adopted the best subset selection method using lasso regression, as implemented in the SmulTCan app (Ozhan et al., 2021). PI values revealed (through K-M analyses) the effective discriminators of prognostic outcomes (Table 4 for OS and DSS; Table 5 for DFS and PFS) for several of the 15 TCGA datasets for which a best subset could be found. We emphasized below only those having highly significant K-M values.

The *SLIT3-ROBO2* pair appeared in the K-M analysis of KIRP, acting opposingly, whereby *SLIT3* contributed to higher risk and *ROBO2* contributed to lower risk for OS, DSS, and PFS. K-M plots of KIRP in Figure 5 indicated significant differentiation between prognostic outcomes for three of four survival types. K-M analyses also produced one of the best outcomes for the KIRC dataset (Fig. 6) with the strong separation of low- and high-risk outcomes and minimal overlap of their confidence intervals particularly for PFS (Fig. 6c).

Low-to-high risk ratios of KIRC for the antagonistic Slit-Robo pair were in the range of 0.34–0.51 with AUC% ± SE% scores of PIs = 67.69 ± 2.96, 70.71 ± 3.25, and 63.56 ± 3.06 for OS, DSS, and PFS, respectively. High *ROBO4* expression's protective effect was once again revealed in the K-M analyses, where the gene contributed to lower risk prognosis in KIRC for OS, DSS, and PFS acting opposingly to *ROBO3* (Tables 4 and 5).

SLIT1 was the only contributing gene to the PIs calculated for LGG and UCEC, but indicated a lower risk in LGG and a higher one in UCEC. K-M plots of LGG for the four survival types indicated a significantly large AUC with *SLIT1*, also exhibiting one of the highest significances ($p < 0.001$ for

Table 4. Slit-Robo Best Subset Members and Corresponding Coefficients Obtained with Lasso Analysis of Each Dataset for OS and DSS Are Listed

	OS						*DSS*					
	K-M p-*value*	*HR of low:high risk*	*HR* p-*value*	*PI coeffs*	*Genes*	*AUC% ± SE% of PI*	*K-M* p-*value*	*HR of low:high risk*	*HR* p-*value*	*PI coeffs*	*Genes*	*AUC% ± SE% of PI*
ACC	0.02	0.38	0.02	−0.08	*SLIT3*	59.77 ± 7.96	0.15×10^{-2}	0.25	0.32×10^{-2}	0.06, 0.05, −0.14	*ROBO1*, *SLIT2*, *SLIT3*	64.20 ± 8.03
KICH	0.06	0.25	0.09	−0.44	*ROBO4*	79.10 ± 7.54	0.18	0.34	0.2	−0.37	*ROBO4*	77.92 ± 8.44
KIRC	0.46×10^{-9}	0.38	0.19×10^{-8}	0.19, −0.08	*ROBO3*, *ROBO4*	67.69 ± 2.96	0.1×10^{-6}	0.34	0.38×10^{-6}	0.26, −0.19	*ROBO3*, *ROBO4*	70.71 ± 3.25
KIRP	0.21×10^{-2}	0.37	0.31×10^{-2}	−0.03, 0.15	*ROBO2*, *SLIT3*	77.06 ± 5.74	0.14×10^{-4}	0.11	0.34×10^{-3}	−0.16, 0.38	*ROBO2*, *SLIT3*	83.54 ± 4.67
LGG	0.23×10^{-5}	0.42	0.44×10^{-5}	−0.18	*SLIT1*	72.69 ± 3.66	0.14×10^{-4}	0.43	0.23×10^{-4}	−0.18	*SLIT1*	73.28 ± 3.74
LUSC	—	—	—	—	—	—	0.02	0.59	0.02	−0.07, −0.04, 0.01	*ROBO1*, *ROBO3*, *SLIT2*	54.54 ± 4.27
MESO	0.04	0.62	0.04	0.03	*ROBO1*	65.69 ± 6.02	—	—	—	—	—	—
PCPG	0.15	0.23	0.19	−0.32	*ROBO4*	82.79 ± 6.84	—	—	—	—	—	—
UCEC	0.47×10^{-3}	0.46	0.64×10^{-3}	0.03	*SLIT1*	55.84 ± 4.30	0.35×10^{-2}	0.46	0.44×10^{-2}	0.04	*SLIT1*	57.50 ± 4.58
UVM	0.16×10^{-4}	0.11	0.35×10^{-3}	−0.01, −0.11, 0.03	*ROBO1*, *ROBO3*, *SLIT1*	64.29 ± 7.59	0.18×10^{-5}	0.07	0.29×10^{-3}	−0.04, −0.05, 0.08	*ROBO1*, *ROBO3*, *SLIT1*	63.95 ± 7.61

Low:high risk HRs and their corresponding *p*-values, as well as the *p*-value of the K-M analysis results based on the PI calculated from the coefficients of each dataset are also given. Refer to Supplementary Table S1 for cancer dataset abbreviations.

AUC, area under the receiver operating characteristic (ROC) curve; K-M, Kaplan–Meier; PI, prognostic index; SE%, standard error %.

TABLE 5. SLIT-ROBO BEST SUBSET MEMBERS AND CORRESPONDING COEFFICIENTS OBTAINED WITH LASSO ANALYSIS OF EACH DATASET FOR DFS AND PFS ARE LISTED

	DFS						*PFS*					
	K-M p-*value*	*HR of low:high risk*	*HR* p-*value*	*PI coeffs*	*Genes*	*AUC% ± SE% of PI*	*K-M* p-*value*	*HR of low:high risk*	*HR* p-*value*	*PI coeffs*	*Genes*	*AUC% ± SE% of PI*
ACC	—	—	—	—	—	—	0.42×10^{-5}	0.22	0.24×10^{-4}	0.95×10^{-1}, 0.02	*ROBO1*, *SLIT2*	76.38 ± 5.66
CHOL	0.34×10^{-2}	0.09	0.02	−0.13	*SLIT3*	76.90 ± 11.70	—	—	—	—	—	—
COAD	0.30×10^{-4}	0.09	0.98×10^{-3}	0.12, 0.11	*ROBO1*, *SLIT1*	71.85 ± 6.05	—	—	—	—	—	—
KICH	—	—	—	—	—	—	0.09	0.34	0.11	0.08	*ROBO2*	72.56 ± 9.51
KIRC	—	—	—	—	—	—	0.35×10^{-4}	0.51	0.48×10^{-4}	0.16, −0.04	*ROBO3*, *ROBO4*	63.56 ± 3.06
KIRP	—	—	—	—	—	—	0.11×10^{-3}	0.34	0.23×10^{-3}	−0.04, 0.17	*ROBO2*, *SLIT3*	68.31 ± 4.77
LGG	0.78×10^{-3}	0.2	0.02×10^{-1}	0.59, −0.13, −0.21	*ROBO3*, *SLIT1*, *SLIT3*	81.36 ± 6.55	0.98×10^{-4}	0.57	0.12×10^{-3}	−0.09	*SLIT1*	71.35 ± 2.89
LUSC	0.02	0.54	0.02	0.02	*SLIT2*	63.24 ± 4.64	—	—	—	—	—	—
PAAD	0.02	0.36	0.02	0.06, 0.01, -0.95×10^{-1}, 0.11	*ROBO1*, *ROBO2*, *SLIT1*, *SLIT2*	62.38 ± 9.11	—	—	—	—	—	—
STAD	0.06	0.56	0.06	0.13, −0.03, 0.02	*ROBO3*, *ROBO4*, *SLIT2*	59.74 ± 5.04	—	—	—	—	—	—
THCA	—	—	—	—	—	—	0.41×10^{-2}	0.43	0.53×10^{-2}	−0.11, −0.04	*ROBO4*, *SLIT3*	63.88 ± 4.57
UVM	—	—	—	—	—	—	0.51×10^{-4}	0.19	0.03×10^{-2}	0.11	*SLIT1*	75.07 ± 6.59

Low:high risk HRs and their corresponding *p*-values, as well as the *p*-value of the K-M analysis results based on the PI calculated from the coefficients of each dataset are also given. Refer to Supplementary Table S1 for cancer dataset abbreviations.

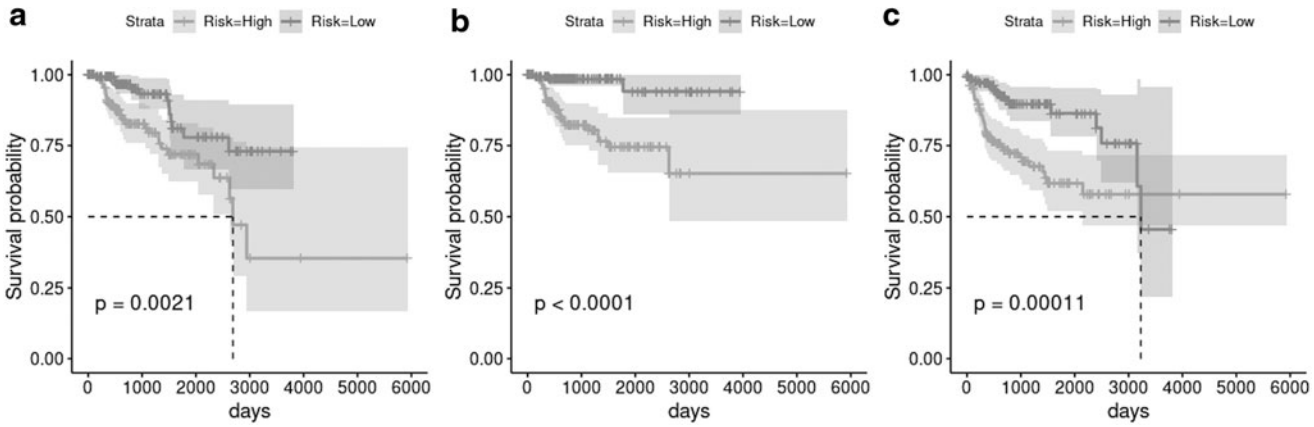

FIG. 5. K-M plots of KIRP for **(a)** OS, **(b)** DSS, and **(c)** PFS. Low- and high-risk prognostic outcomes significantly differentiated based on the median PI for each survival type. K-M, Kaplan–Meier; PI, prognostic index.

Fig. 7a–d; Tables 4 and 5). While *SLIT3* contributed to lower risk in TCHA-CHOL, *ROBO1* and *SLIT1* led to a higher risk in COAD (AUC% ± SE% values of the PIs were 76.90 ± 11.70 and 71.85 ± 6.05 for CHOL and COAD, respectively). Other K-M plots for significant differentiation between risk groups were for OS in MESO (see also Supplementary Fig. S25 for the forest plot), for DFS in PAAD, for OS, DSS, and PFS in ACC and UVM, and for DFS in KICH (Tables 4 and 5).

Discussion

A prognostic HR GS refers to the expression pattern of a group of genes associated with the tumor prognosis and presents great potential for improving the prediction of survival rates (Wang et al., 2017). The role of axon guidance cues of the nervous system on cancer progression and prognosis has previously been emphasized (Hao et al., 2020; Ozhan et al., 2021). In this study we discovered independent HR GSs as pairs/modules of the Slit-Robo axon guidance gene family that can predict survival significantly across TCGA-PANCAN datasets. Moreover, we have demonstrated that the multivariable Cox survival analysis more frequently resulted in the independent pairing between Slits and Robo rather than only Robo-Robo or only Slit-Slit pairing.

We also were able to identify several recurrent signatures within different cancers; hence, these novel cancer-specific yet independent Slit-Robo pairs and/or modules we identified could provide promising leads for further tests. Consequently, we propose that such co-dependent ligand/receptor interactions, as in the case of Slit-Robo molecules, should be investigated with multivariable regression, applied to the whole family, without first filtering with univariable regression.

Our results further corroborated the importance of Slit-Robo in kidney cancers such that *ROBO3*, *ROBO4*, and/or *SLIT3* were strongly associated with all three of kidney cancers. KIRC and KIHC were more similar to each other than they were to KIRP, which shared prognostic similarities with BRCA. The observed compartmentalization of Slit-Robo members in kidney cancers other than *ROBO4* might indicate the different histological characteristics of clear, papillary, and chromophobe renal cell carcinomas and the differential level of expression of Slit-Robo members across their respective tissues.

The protective profile of *ROBO4* by itself across many of the investigated TCGA cancer datasets, including the pheochromocytoma and paraganglioma dataset, TCGA-PCPG of neuronal origin, could also be attributed to *ROBO4*'s angiogenesis-inhibiting properties, demonstrated in wound healing experiments (Zhang et al., 2016). A previous independent study has also indicated a lower *ROBO4* in liver

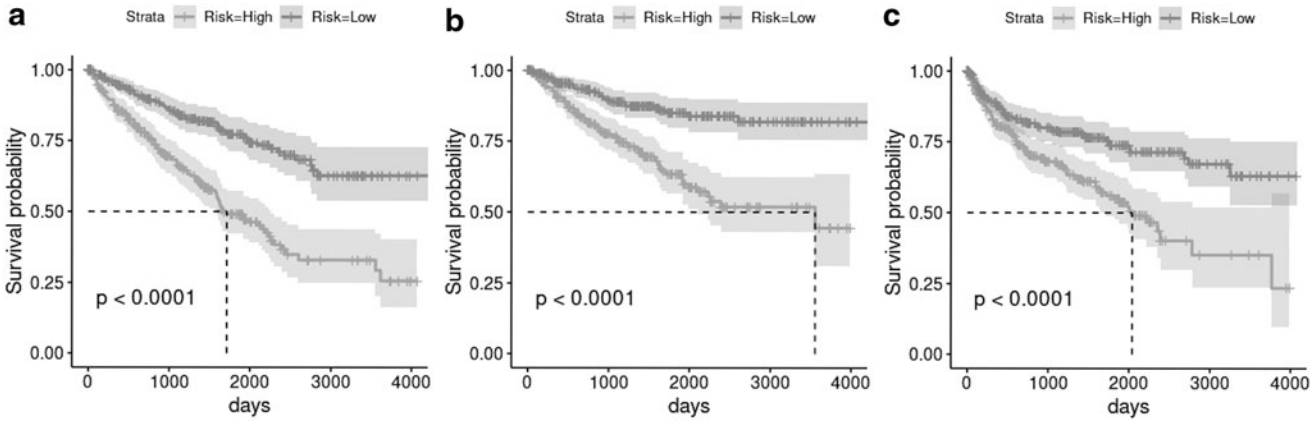

FIG. 6. K-M plots of KIRC for **(a)** OS, **(b)** DSS, and **(c)** PFS. Low- and high-risk prognostic outcomes significantly differentiated based on the median PI for each survival type.

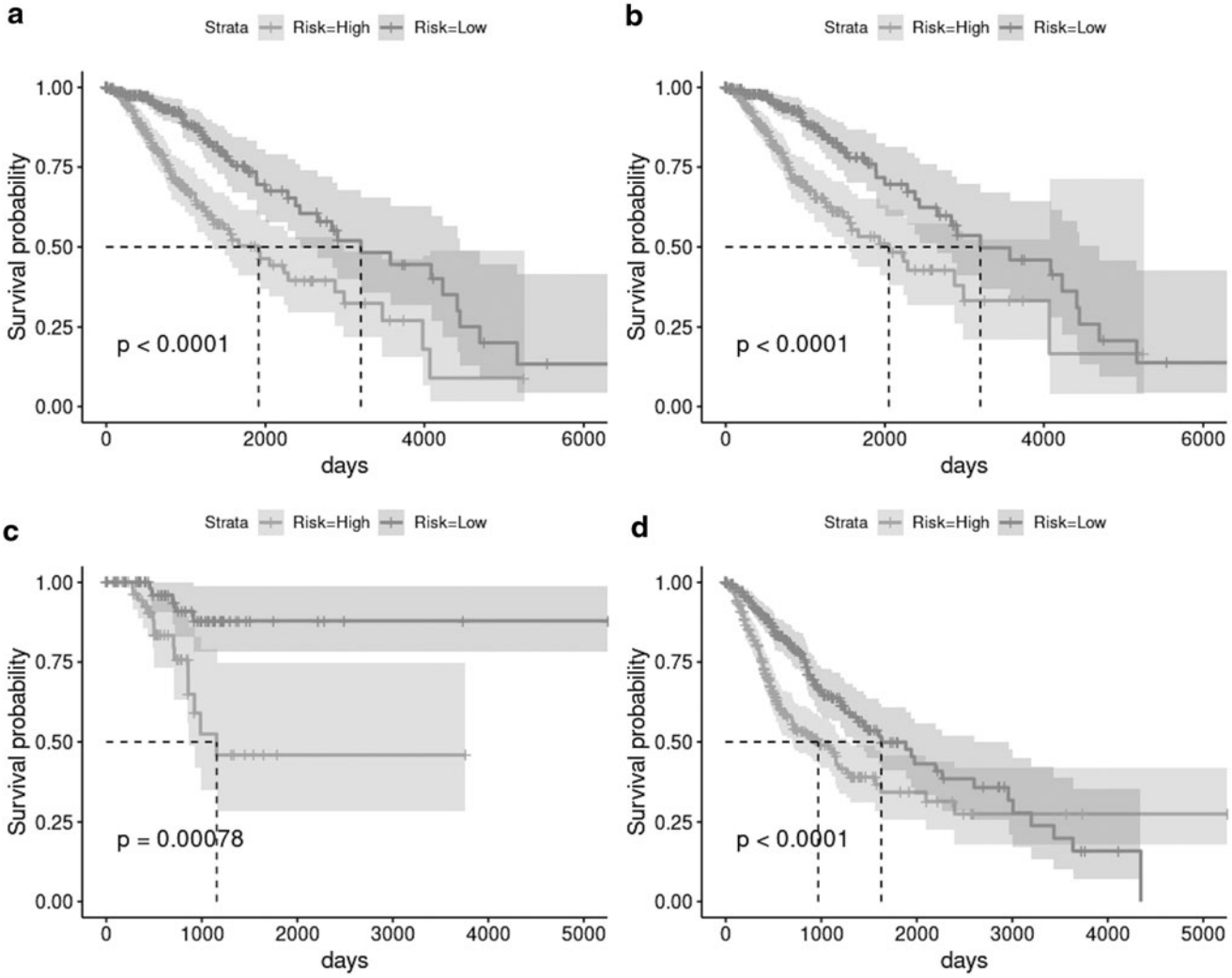

FIG. 7. K-M plots of LGG for **(a)** OS, **(b)** DSS, **(c)** DFS, and **(d)** PFS. Low- and high-risk prognostic outcomes significantly differentiated based on the median PI for each survival type.

tumors (Avci et al., 2008), which our multivariable Cox regression analysis supported this with approaching significance in TCGA-LIHC.

Our results show that Slit-Robo pathway expression, when analyzed with multivariable Cox regression, has revealed other novel prognostic members of the pathway. One such example is the lung adenocarcinoma (LUAD) in which previous studies implicated *SLIT2* expression (Rezniczek et al., 2019) that was shown to inhibit migration (Kong et al., 2015) and considered a tumor suppressor (Zhang et al., 2015). However, our analysis with LUAD, based on the whole Slit-Robo gene family, did not implicate *SLIT2* as prognostic, but instead revealed *ROBO2*'s higher expression as a marker for poor prognosis, for three different survival types, that is, OS, DSS, and PFS.

ROBO2 has been previously shown to be decreased in prostate cancer as well, but was found to be upregulated in inflammatory breast cancer (Bieche et al., 2004; Dickinson et al., 2004); and our study is the first implicating increased *ROBO2* expression, independent of its relationship to the other Slit-Robo members, in the prognosis of LUAD patients.

In our analysis, *SLIT3* was the most significantly associated with poorer prognosis in BRCA, while independently, higher levels of *ROBO2* were significantly better prognostically, supporting previous findings (Yuasa-Kawada et al., 2009). Previously, *SLIT3* has been found to be a tumor suppressor in lung cancer cells whose silencing increases metalloproteinase activity (Zhang et al., 2015); however, in connection with reduced levels of *ROBO2*, *SLIT3* could be an oncogene in BRCA.

Previous studies have also shown that specific Slit-Robo members acting in pairs are involved in various cellular functions and disorders other than cancer as previously introduced. Our HR_{multi} analysis demonstrated the presence of known Slit-Robo pairs also with impacts on cancer survival, not possible to extract otherwise, that is, using univariable Cox regression alone. For instance, our study showed that several well-known pairs from literature were associated with cancers, that is, the *SLIT3-ROBO4* pair (Paul et al., 2013), with KIRP; the *SLIT2-ROBO3* pair (Cariboni et al., 2012), with BLCA; the *SLIT2-ROBO4* pair (Jones et al., 2009), with KICH; and the *SLIT2-ROBO1* pair (Qin et al., 2015), with ACC.

Furthermore, in our analysis, many Slit-Robo pairs acted antagonistically. For instance, high expression of *SLIT2* and lower expression of *ROBO1* were hazardous for DSS in LUSC, DLBC, and THCA datasets. Other antagonistic pairs included the *SLIT3-ROBO2* pair in KIRP for OS, DSS, and PFS; the *SLIT3-ROBO3* pair in OV for DSS; and the *SLIT1-ROBO2* pair in UCEC for DSS. In all of these, Slits had higher expression, while Robos had lower expression, and together they were associated with poor prognosis. It is tempting to speculate that these antagonistic pairs are likely to work together, while their individual expressions balance one another. Accordingly, the emerging role of antagonistic Slit-Robo pairs in cancer prognosis can be investigated further experimentally due to their novelty.

Conclusion

Univariable analyses helped compare the impacts of Slit-Robo members on each dataset across TCGA-PANCAN and identify which cancer types were more significantly affected by Slit-Robo alterations. However, the multivariable Cox regression was required to identify the independent Slit-Robo pairs and/or modules with significant HR signatures in cancer- as well as survival-specific manners.

Our study provided AUC% calculations of all the multivariable Slit-Robo models in the study for all four survival types (Supplementary Table S3), which could serve as a reference in future studies. Our results suggested higher expressions of *SLIT1*, *SLIT2*, and *SLIT3* could be associated with poor prognosis when coupled with lower levels of expression in one or more Robos, although the opposite patterns also were detected. Moreover, KIRP and BRCA; BLCA and LUSC; and KIRC and KICH showed similar Slit-Robo HR profiles and/or best Slit-Robo subsets.

Our findings implicate that significantly associated members of the ligand-receptor pathways, as in the case of Slit-Robo pathway, should be tested as a family to better understand if they can be used in potential therapeutic applications. Our analyses further suggest that unique Slit-Robo pairs/modules, commonly exhibiting antagonistic patterns for DSS, exist among different cancers that can be used to differentiate between prognostic outcomes, that is, low or high risk. Furthermore, our methodology can easily be applied to other ligand-receptor pathways and/or gene sets known to act in pairs or modules to reveal novel HR GSs and determine how specific subsets of each pathway's members could be used to predict prognostic outcomes.

Availability of Data

The Slit-Robo TSV file obtained from UCSC Xena is available as a supplemental file (Supplementary Data S1). Matrices generated from the coxph() HR calculations in this article can be found in the Supplementary Tables S4–S20. Forest plots of datasets mentioned in the text, for all analyzable survival types, can be found in Supplementary Figures S5–S25.

Code Availability

Code used in this research will be made available upon request to the authors.

Author Disclosure Statement

The authors declare they have no conflicting financial interests.

Funding Information

This research did not receive any specific grant or funding.

Supplementary Material

Supplementary Figure S1
Supplementary Figure S2
Supplementary Figure S3
Supplementary Figure S4
Supplementary Figure S5
Supplementary Figure S6
Supplementary Figure S7
Supplementary Figure S8
Supplementary Figure S9
Supplementary Figure S10
Supplementary Figure S11
Supplementary Figure S12
Supplementary Figure S13
Supplementary Figure S14
Supplementary Figure S15
Supplementary Figure S16
Supplementary Figure S17
Supplementary Figure S18
Supplementary Figure S19
Supplementary Figure S20
Supplementary Figure S21
Supplementary Figure S22
Supplementary Figure S23
Supplementary Figure S24
Supplementary Figure S25
Supplementary Table S1
Supplementary Table S2
Supplementary Table S3
Supplementary Table S4
Supplementary Table S5
Supplementary Table S6
Supplementary Table S7
Supplementary Table S8
Supplementary Table S9
Supplementary Table S10
Supplementary Table S11
Supplementary Table S12
Supplementary Table S13
Supplementary Table S14
Supplementary Table S15
Supplementary Table S16
Supplementary Table S17
Supplementary Table S18
Supplementary Table S19
Supplementary Table S20
Supplementary Data S1

References

Avci ME, Konu O, and Yagci T. (2008). Quantification of SLIT-ROBO transcripts in hepatocellular carcinoma reveals two groups of genes with coordinate expression. BMC Cancer 8, 392.

Bieche I, Lerebours F, Tozlu S, Espie M, Marty M, and Lidereau R. (2004). Molecular profiling of inflammatory

breast cancer: Identification of a poor-prognosis gene expression signature. Clin Cancer Res 10, 6789–6795.
Blockus H, and Chedotal A. (2016). Slit-Robo signaling. Development 143, 3037–3044.
Blum A, Wang P, and Zenklusen JC. (2018). SnapShot: TCGA-analyzed tumors. Cell 173, 530.
Cariboni A, Andrews WD, Memi F, et al. (2012). Slit2 and Robo3 modulate the migration of GnRH-secreting neurons. Development 139, 3326–3331.
Carr L, Parkinson DB, and Dun XP. (2017). Expression patterns of Slit and Robo family members in adult mouse spinal cord and peripheral nervous system. PLoS One 12, e0172736.
Chen H, Xu C, Yu Q, et al. (2021). Comprehensive landscape of STEAP family functions and prognostic prediction value in glioblastoma. J Cell Physiol 236, 2988–3000.
Choi YJ, Yoo NJ, and Lee SH. (2014). Down-regulation of ROBO2 expression in prostate cancers. Pathol Oncol Res 20, 517–519.
Dickinson RE, Dallol A, Bieche I, et al. (2004). Epigenetic inactivation of SLIT3 and SLIT1 genes in human cancers. Br J Cancer 91, 2071–2078.
Galili T, O'callaghan A, Sidi J, and Sievert C. (2018). heatmaply: An R package for creating interactive cluster heatmaps for online publishing. Bioinformatics 34, 1600–1602.
Gao GF, Parker JS, Reynolds SM, et al. (2019). Before and after: Comparison of legacy and harmonized TCGA genomic data commons' data. Cell Syst 9, 24–34.
Gerds TA, and Ozenne B. (2020). riskRegression: Risk Regression Models and Prediction Scores for Survival Analysis with Competing Risks. https://CRAN.R-project.org/package=riskRegression/. Last accessed January 15, 2021.
Goldman MJ, Craft B, Hastie M, et al. (2020). Visualizing and interpreting cancer genomics data via the Xena platform. Nat Biotechnol 38, 675–678.
Hao W, Yu M, Lin J, et al. (2020). The pan-cancer landscape of netrin family reveals potential oncogenic biomarkers. Sci Rep 10, 5224.
Ho TH, Serie DJ, Parasramka M, et al. (2017). Differential gene expression profiling of matched primary renal cell carcinoma and metastases reveals upregulation of extracellular matrix genes. Ann Oncol 28, 604–610.
Jones CA, Nishiya N, London NR, et al. (2009). Slit2-Robo4 signalling promotes vascular stability by blocking Arf6 activity. Nat Cell Biol 11, 1325–1331.
Kassambara A. (2020). ggpubr: 'ggplot2' Based Publication Ready Plots. https://CRAN.R-project.org/package=ggpubr/. Last accessed August 10, 2020.
Kassambara A, Kosinski M, and Biecek P. (2020). Survminer: Drawing Survival Curves Using 'ggplot2'. https://CRAN.R-project.org/package=survminer/. Last accessed September 17, 2020.
Kong R, Yi F, Wen P, et al. (2015). Myo9b is a key player in SLIT/ROBO-mediated lung tumor suppression. J Clin Invest 125, 4407–4420.
Lu X, Zhou Y, Meng J, et al. (2020). RNA processing genes characterize RNA splicing and further stratify colorectal cancer. Cell Prolif 53, e12861.
Meng Z, Ren D, Zhang K, Zhao J, Jin X, and Wu H. (2020). Using ESTIMATE algorithm to establish an 8-mRNA signature prognosis prediction system and identify immunocyte infiltration-related genes in Pancreatic adenocarcinoma. Aging (Albany NY) 12, 5048–5070.
Neuwirth E. (2014). RColorBrewer: ColorBrewer Palettes. https://CRAN.R-project.org/package=RColorBrewer/. Last accessed March 20, 2021.
Ozhan A, Tombaz M, and Konu O. (2021). SmulTCan: A Shiny application for multivariable survival analysis of TCGA data with gene sets. Comput Biol Med 137, 104793.
Paul JD, Coulombe KLK, Toth PT, et al. (2013). SLIT3-ROBO4 activation promotes vascular network formation in human engineered tissue and angiogenesis in vivo. J Mol Cell Cardiol 64, 124–131.
Qin F, Zhang H, Ma L, et al. (2015). Low expression of Slit2 and Robo1 is associated with poor prognosis and brain-specific metastasis of breast cancer patients. Sci Rep 5, 14430.
Rezniczek GA, Grunwald C, Hilal Z, et al. (2019). ROBO1 expression in metastasizing breast and ovarian cancer: SLIT2-induced chemotaxis requires heparan sulfates (heparin). Anticancer Res 39, 1267–1273.
Schmid BC, Rezniczek GA, Fabjani G, Yoneda T, Leodolter S, and Zeillinger R. (2007). The neuronal guidance cue Slit2 induces targeted migration and may play a role in brain metastasis of breast cancer cells. Breast Cancer Res Treat 106, 333–342.
Stadler K. (2018). Cultevo: Tools, Measures and Statistical Tests for Cultural Evolution. https://kevinstadler.github.io/cultevo/. Last accessed November 15, 2020.
Therneau TM, and Grambsch PM. (2000). Modeling survival data: Extending the Cox model. In: *Statistics for Biology and Health*. New York: Springer, pp. 1 online resource (xiii, 350 pages).
Tong M, Jun T, Nie Y, Hao J, and Fan D. (2019). The role of the Slit/Robo signaling pathway. J Cancer 10, 2694–2705.
Wang S, and Liu X. (2019). The UCSCXenaTools r Package: A toolkit for accessing genomics data from UCSC Xena platform, from cancer multi-omics to single-cell RNA-Seq. J Open Source Softw 4, 4750.
Wang Y, Goodison S, Li X, and Hu H. (2017). Prognostic cancer gene signatures share common regulatory motifs. Sci Rep 7, 4750.
Warnes GR, Bolker B, and Lumley T. (2020). gtools: Various R Programming Tools. https://CRAN.R-project.org/package=gtools/. Last accessed November 22, 2020.
Wickham H. (2016). *ggplot2: Elegant Graphics for Data Analysis*. New York: Springer-Verlag.
Wu JY, Feng L, Park HT, et al. (2001). The neuronal repellent Slit inhibits leukocyte chemotaxis induced by chemotactic factors. Nature 410, 948–952.
Wu L, Quan W, Luo Q, Pan Y, Peng D, and Zhang G. (2020). Identification of an immune-related prognostic predictor in hepatocellular carcinoma. Front Mol Biosci 7, 567950.
Xia Y, Wang L, Xu Z, et al. (2019). Reduced USP33 expression in gastric cancer decreases inhibitory effects of Slit2-Robo1 signalling on cell migration and EMT. Cell Prolif 52, e12606.
Xue M, Shang J, Chen B, et al. (2019). Identification of prognostic signatures for predicting the overall survival of uveal melanoma patients. J Cancer 10, 4921–4931.
Yuasa-Kawada J, Kinoshita-Kawada M, Rao Y, and Wu JY. (2009). Deubiquitinating enzyme USP33/VDU1 is required for Slit signaling in inhibiting breast cancer cell migration. Proc Natl Acad Sci U S A 106, 14530–14535.
Zhang C, Guo H, Li B, et al. (2015). Effects of Slit3 silencing on the invasive ability of lung carcinoma A549 cells. Oncol Rep 34, 952–960.
Zhang F, Prahst C, Mathivet T, et al. (2016). The Robo4 cytoplasmic domain is dispensable for vascular permeability and neovascularization. Nat Commun 7, 13517.

Zhou WJ, Geng ZH, Chi S, et al. (2011). Slit-Robo signaling induces malignant transformation through Hakai-mediated E-cadherin degradation during colorectal epithelial cell carcinogenesis. Cell Res 21, 609–626.

Address correspondence to:
Ozlen Konu, PhD
Department of Molecular Biology and Genetics
Bilkent University
Ankara 06800
Turkey

E-mail: konu@fen.bilkent.edu.tr

Abbreviations Used

AUC = area under the receiver operating characteristics (ROC) curve
DFS = disease-free survival
DSS = disease-specific survival
GnRH = Gonadotropin-releasing hormone
HR = hazard ratio
K-M = Kaplan–Meier
OS = overall survival
PFS = progression-free survival
PI = prognostic index
SE = standard error
TCGA = The Cancer Genome Atlas